P58330.1

ENERGY BALANCE OVER THE TROPICAL ATLANTIC OCEAN

Amauri P. de Oliveira *, Jacyra Soares, Sarasvati A. Bacellar, Antonio J. Machado and América M. Espinosa
Institute of Astronomy, Geophysics and Atmospheric Sciences, University of São Paulo

1. INTRODUCTION

The climate change issues have brought up attention to the scarcity of information about the short-term variation of ocean-atmosphere interactions. Discrepancies between climate models are known worldwide and are particularly important over the tropical and subtropical regions of the Atlantic Ocean in the Southern Hemisphere. Climate models diverge about the intensity of the heat, moisture and momentum fluxes between atmosphere and ocean (Wainer *et al*., 2002). Observations in the area are not available with the time and space resolution required. Very few observational works have been carried out in the Southern Atlantic Ocean (Dourado and Oliveira, 2001).

The present work is a description of the observations carried out on May 15-24, 2002, as part of the FluTuA Program (Soares *et al.* 2001). These observations were carried out on board of the Brazilian Navy Ship (Comte. Manhães) between Natal (6^0S, 35.2^0W) and Arquipelago de São Pedro e São Paulo (1^0N, 29.3^0W).

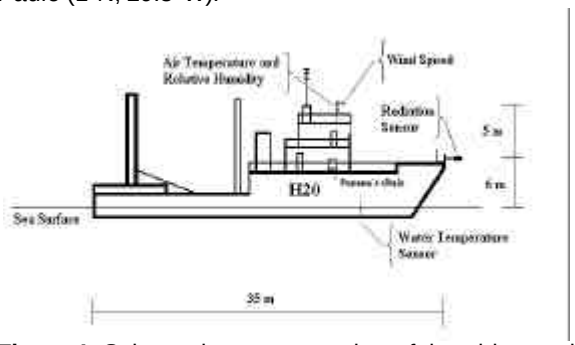

Figure 1: Schematic representation of the ship used to carry out the measurements over the Atlantic Ocean. The ship, called *Manhães,* is a military vessel used by the Brazilian Navy to launch buoys in the ocean.

2. OBSERVATIONS

The observations were carried out on board of the Brazilian Navy ship Manhães (Figure 1). The ship was set up with wind velocity sensors, air temperature and relative humidity sensors, radiation sensor and water temperature sensor. The characteristic of each sensor is described in Table 1. This sensors were connected to the data acquisition system Datalogger 21X, manufactured by Campbell Inc. The sampling rate was set equal to 0.2 Hz and 5 minutes average was calculated for all variables.

*Corresponding author address: Amauri Oliveira, Univ. of São Paulo, Dept. of Atmospheric Sciences, Rua do Matão, 1226, São Paulo, 05508-900, SP, Brazil; email: apdolive@usp.br.

Table 1: Sensor characteristics.

Sensor	*Manufacturer*	*Accuracy*
Net Radiometer, model CNR 1	Kipp and Zonen	2.5%
Anemometer Gill Propeller, model 27106	R.M. Yong	1%
Temperature and relative humidity model HMP45C	Vaisala	0.1ºC and 2 %
Water temperature, Vaisala, model 107	Vaisala	± 0,1 ºC

The net radiation sensor was set up in the up front of the vessel, about 1 meter far from the ship, and 6 meters above the sea surface. The air temperature and relative humidity sensors were set up at the upper level of the ship, near the wind sensors, at 11 meters above the sea surface. Two anemometers were set up in the boom located at the upper level of the ship, also 11 m above the sea surface. The anemometers were oriented in the direction parallel and perpendicular to the ship (Figure 1).

The position of the ship was obtained from an onboard GPS system. The trajectory carried by the ship was built from the GPS information (Figure 2). This information was also used to estimate the ship velocity and orientation. The ship orientation corresponds to the angle formed between the ship and east-west direction.

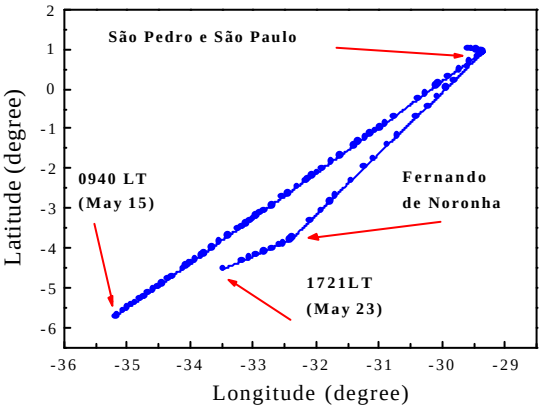

Figure 2: Trajectory described by the Manhães during the observational campaign carried out between May 15 and 23, 2002.

The wind velocity and direction was evaluated using the wind velocity measured on board of the ship and

the ship velocity and direction evaluated from the GPS information, using the expressions:

$$u_S = u' \cos A_S - v' \sin A_S \quad (1)$$

$$v_S = u' \sin A_S + v' \cos A_S \quad (2)$$

where u' and v' are, respectively, the wind components perpendicular and parallel to the ship, measured by the propeller anemometer, and A_S is the ship orientation angle.

3. RESULTS

The observational data and some empirical expressions used to evaluate the energy fluxes are addressed here. As example, the results obtained for year day 136 (May, 16) are discussed.

3.1 Shortwave Radiation

The solar radiation at the top of the atmosphere was estimated using the expression:

$$I_0 = S_0 (d_m / d)^2 \cos\gamma \quad (3)$$

where d_m is the average distance between the Sun and the Earth, d is the actual Sun-Earth distance, γ is the solar zenithal angle calculated from:

$$\cos(\gamma) = \text{sen}(\delta)\text{sen}(\phi) + \cos(\delta)\cos(\phi)\text{sen}(h) \quad (4)$$

where, δ is the sun declination, ϕ is the latitude and h is the hourly angle. The solar declination is evaluated from the expression:

$$\delta = a_1 + a_2 \cos(\theta) + a_3 \text{sen}(\theta) + a_4 \cos(2\theta) + a_5 \text{sen}(2\theta) \quad (5)$$

where the constants are indicated in Table 2 and $\theta = 2\pi d/365$ is calculated in terms of year day (d = 0 January first and 364 for December 31). Similarly, the Sun-Earth distance varies in terms of the time of the year as:

$$d = b_1 + b_2 \cos(\theta) + b_3 \text{sen}(\theta) + b_4 \cos(2\theta) + b_5 \text{sen}(2\theta) \quad (6)$$

Table 2: Polynomial coefficients used to estimate the solar declination and the Sun-Earth distance.

a_1	0.006918	b_1	0,0172
a_2	-0.399912	b_2	0,4281
a_3	0.070257	b_3	-7,3515
a_4	-0.006758	b_4	-3,3495
a_5	0.000908	b_5	-9,3619

The incoming solar radiation, SW_{DW}, at the surface was given by:

$$SW_{DW} = -I_0 T_R \quad (7)$$

where I_0 is the incoming irradiance and T_R is the broadband transmissivity of the atmosphere estimated from:

$$T_R = (0.6 + 0.2\cos\gamma) \quad (8)$$

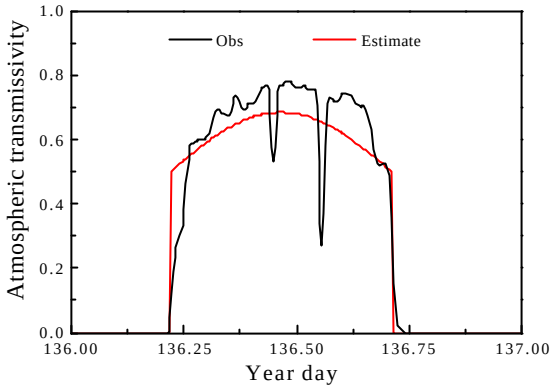

Figure 3: Atmospheric transmissivity as a function of time.

Figure 3 displays the broadband atmospheric transmissivity observed (evaluated as the ratio between the observed global shortwave radiation and the solar radiation at the top of the atmosphere) and estimate by expression (8). The observed atmospheric transmissivity as a function of solar zenithal angle is shown in Figure 4.

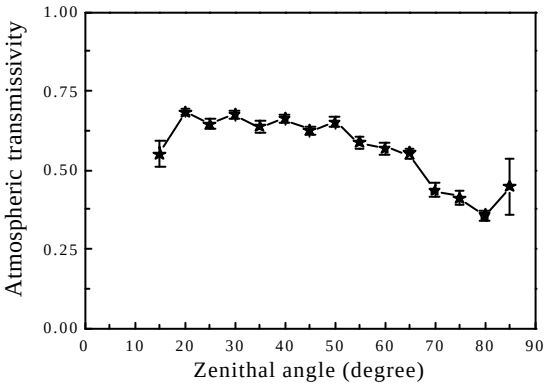

Figure 4: Average atmospheric transmissivity as function of the solar zenithal angle. The vertical bars correspond to the statistical error. Based on observations carried out during the whole campaign.

The outgoing solar radiation, SW_{UP}, was estimated from:

$$SW_{UP} = -\alpha\, SW_{DW} \quad (9)$$

where α is the surface albedo.

Figure 5 shows the average surface albedo as a function of solar zenithal angle, calculated from the solar radiation observations (ratio of outgoing to incoming shortwave radiations). The average albedo for the lower zenithal angles is about 0.06. This value is compatible with the albedo value found by Payne (1972), for conditions of light winds and relatively smooth seas.

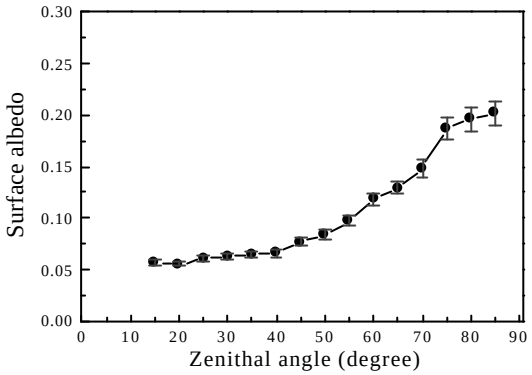

Figure 5: Average surface albedo as function of the solar zenithal angle. The vertical bars correspond to the statistical error. Based on observations carried out during the whole campaign.

The surface albedo for the year day 136 is displayed in Figure 6. The estimated albedo was based on the Fresnel expression proposed by Cogley (1979)

$$\alpha = 0.5\left[\frac{\sin^2(\gamma - r)}{\sin^2(\gamma + r)} + \frac{\tan^2(\gamma - r)}{\tan^2(\gamma + r)}\right] \qquad (10)$$

where $r = \sin^{-1}[(\sin\gamma)/1.33]$.

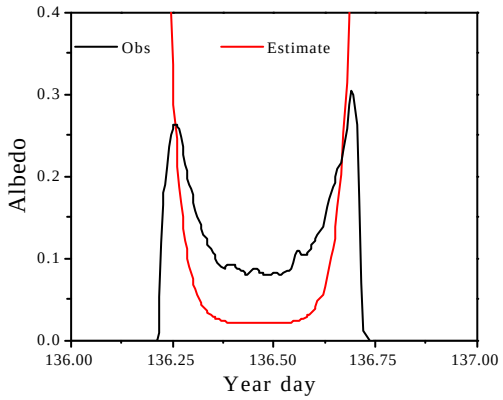

Figure 6: Surface albedo as function of the time.

Figure 7 shows the solar radiation at the top of the atmosphere (estimated by expression 3) and the observed and estimated (by expression 7) incoming shortwave radiations.

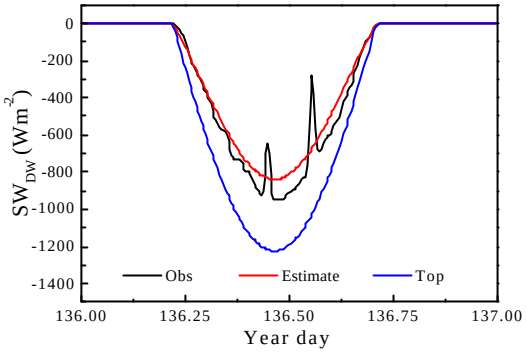

Figure 7: Observed (in black) and estimated (in red) incoming shortwave radiations. The solar radiation at the atmospheric top is displayed in blue line.

The estimated (by expression 12) and observed shortwave outgoing radiations are in Figure 8.

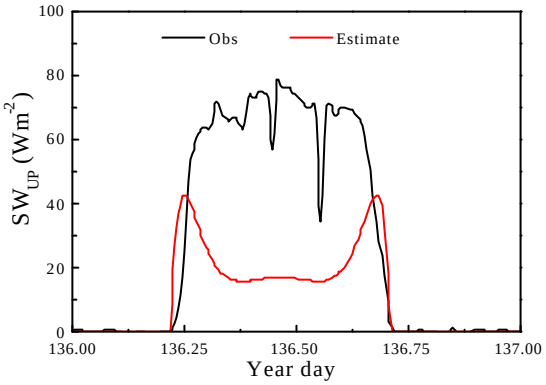

Figure 8: Observed (in black) and estimated (in red) outgoing shortwave radiations.

3.2 Longwave Radiation

The longwave radiation emitted by the surface, LW_{UP}, was calculated from the following expression:

$$LW_{UP} = \varepsilon \sigma T_S^4 \qquad (11)$$

where ε is the surface emissivity, σ is the Stefan-Boltzman constant and T_S is the surface temperature.

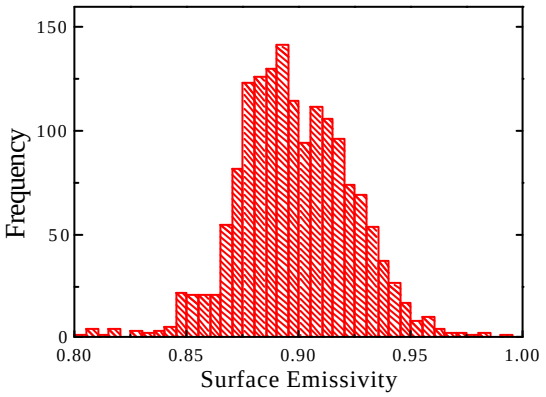

Figure 9: Frequency of surface emissivity values.

The frequency of the surface emissivity values is displayed in Figure 9. The surface emissivity as function of the time is shown in Figure 10.

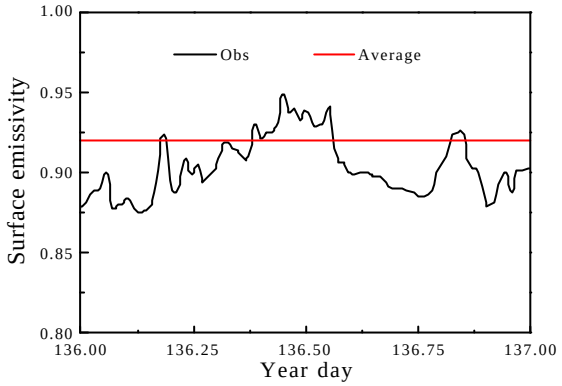

Figure 10: Surface emissivity as function of the time.

Figure 11 shows the observed and estimated (using expression 11, with $\varepsilon = 0.92$) longwave emitted by the surface.

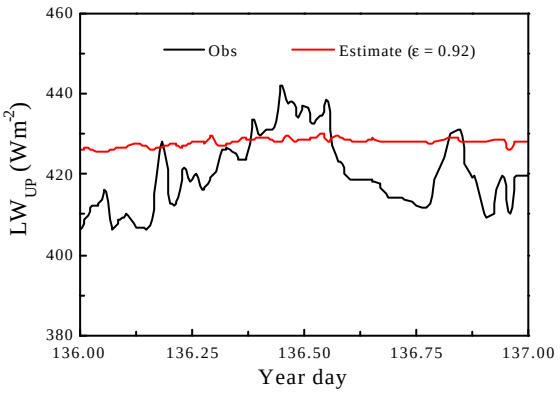

Figure 11: Observed (in black) and estimated (in red) longwave radiation emitted by the surface.

The longwave radiation emitted by the atmosphere, LW_{DW}, was estimated from the following expression:

$$LW_{DW} = -(a+b\sqrt{e})\,\sigma\,T_r^4 \qquad (12)$$

where e is the value of vapor pressure in mb at reference level; a and b were set equal to 0.52 and 0.064, respectively and T_r is the temperature at reference level. This expression is valid for clear days.

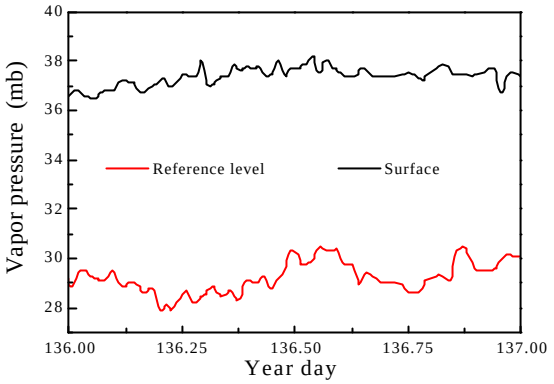

Figure 12: Vapor pressure at reference level (in black) and at the surface (in red).

Figures 12 and 13 show the vapor pressure and temperature at reference level (11 m), for the year day 136. These figures also display the vapor pressure and temperature at the surface.

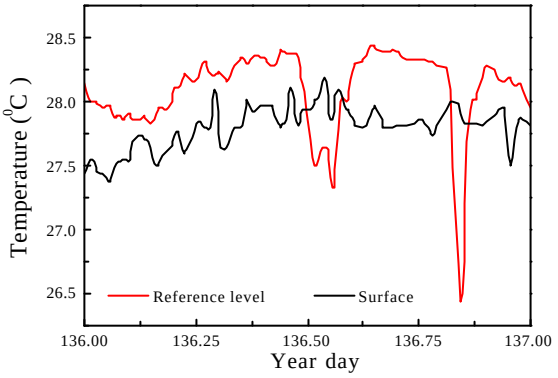

Figure 13: Temperature at reference level (in black) and at the surface (in red).

The observed and estimated (by expression 12) longwave radiation emitted by the atmosphere is shown in Figure 14.

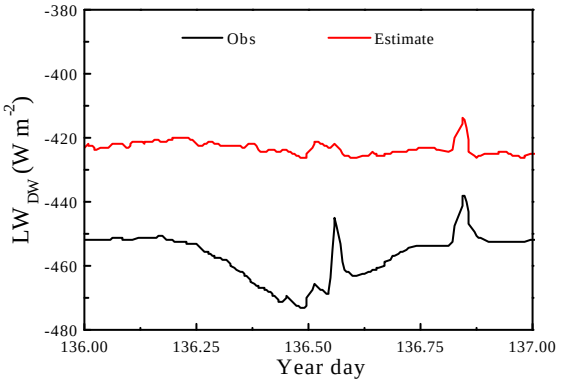

Figure 14: Observed (in black) and estimated (in red) longwave radiation emitted by the atmosphere.

3.3 Radiation Balance

The net radiation, R_N, at the ocean surface was evaluated considering the shortwave (SW) and longwave (LW) atmospheric components at the air-sea interface:

$$R_N = SW_{DW} + SW_{UP} + LW_{DW} + LW_{UP} \quad (13)$$

Figure 15 displays the net radiation observed and estimate as the balance between the longwave and shortwave radiations obtained using expressions (7), (9), (11) and (12).

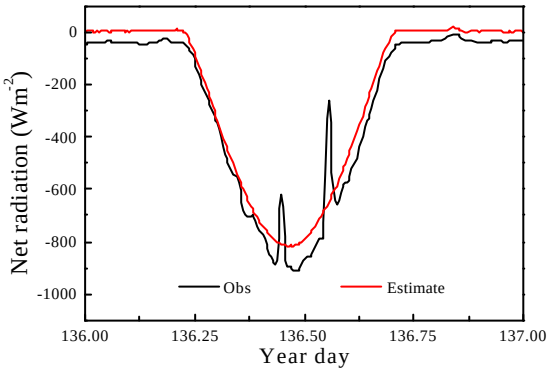

Figure 15: Observed (in black) and estimated (in red) net radiation.

3.4 Energy Balance

The sensible heat flux, H, was estimated as:

$$H = -\rho\, c_p C_H\, V_r (T_s - T_r) \quad (14)$$

where ρ is the air density, c_p is the air specific heat at constant pressure, C_H is the heat exchange coefficient (here, considered equal to 10^{-3}; Smith, 1988), V_r is the wind velocity at reference level, T_s is the surface temperature and T_r the air temperature at reference level. Figure 16 shows the observed wind velocity (V_r) during the year day 136.

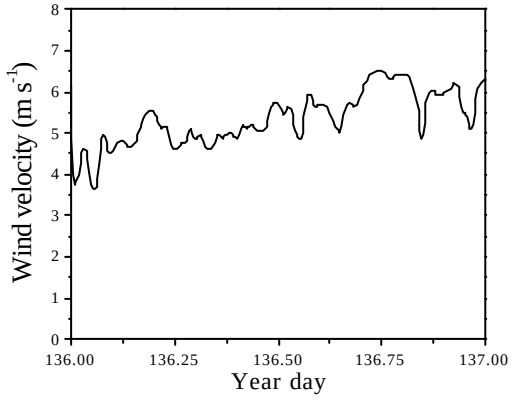

Figure 16: Observed wind velocity.

The latent heat flux, LE, was estimated as:

$$LE = -\rho\, L\, C_E\, V_r\, (q_s - q_r) \quad (15)$$

where, L is the latent heat of evaporation, C_E is the moisture exchange coefficient (here, considered equal to $1.2\ 10^{-3}$; Smith, 1989), q_s is the saturation specific humidity at the surface and q is the air specific humidity at reference level (Figure 17).

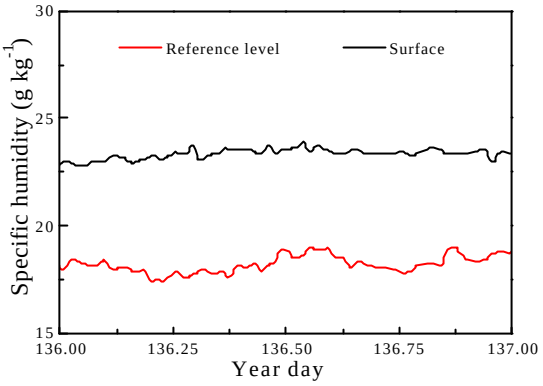

Figure 17: Air specific humidity at reference level (in black) and saturation specific humidity at the surface (in red).

The net heat flux (Q) is the sum of the radiation flux components (expression 13) plus the turbulent flux components (expressions 14 and 15). Here, the ocean looses energy when evaporation occurs and when the sensible heat flux is positive. The energy balance is displayed in Figure 18.

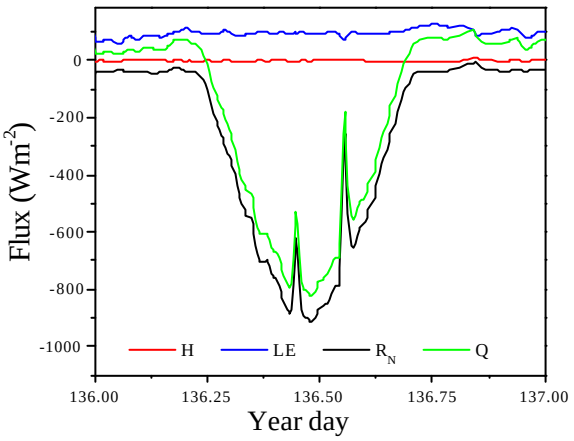

Figure 18: Energy fluxes.

4. CONCLUSION

The observational campaign carried out on May 15-24, 2002, as part of the FluTuA Program, is described here. During 9 days, 5 minute averaged measurements of (a) solar radiation fluxes (incoming and outcoming) and longwave radiation fluxes (atmospheric and surface emission), at 6 m above the

sea level; (b) air temperature, relative humidity and horizontal wind components, at 11 m and (c) sea surface temperature were gathered continuously.

These observations were carried out on board of the Brazilian Navy Ship (*Comte. Manhães*), between Natal (6^0S, 35.2^0W) and Arquipelago de São Pedro e São Paulo (1^0N, 29.3^0W). The data was used to validate empirical expressions currently used to estimate energy components at the surface of the ocean.

Acknowledgments. The first and second authors acknowledge the financial support provided by CNPq, Fapesp, USP/COFECUB (UC 27/96) and CNPq/SCI (910072/00-0). We thank the Brazilian Navy, in special the Comandante Jean Félix de Oliveira and his helpful crew. We also thank Susanna Sichel for her valuable service as an assistant.

5. REFERENCES

Cogley, J.G., 1979: The albedo of water as a function of latitude. *Monthly Weather Review*, **107**, 775-781.

Dourado, M., and Oliveira, A. P., 2001: Observational description of the atmospheric and oceanic boundary layers over the Atlantic Ocean. *Revista Brasileira de Oceanografia,* **49**, 49-64.

Payne, R.E., 1972: Albedo of the sea surface. *J. Atmos. Sci.,* **29**, 959-970.

Smith, S.D., 1988: Coefficients for sea surface wind stress, heat flux, and wind profiles as a function of wind speed and temperature. *J. Geophys. Res*., **93**, 15467-15472.

Smith, S.D., 1989: Water vapor flux at the sea surface. *Boundary-Layer Meteor*., **47**, 277-293.

Soares, J., Oliveira, A. P., Wainer, I., Servain, J., 2001: Turbulent fluxes over the tropical Atlantic Ocean. *Proceedings of the WCRP/SCOR Workshop Intercomparison and Validation of Ocean-Atmosphere Flux Field*, 21-24 May 2001, Washington, DC, EUA, 334-337

Wainer, I., A.Taschetto, J.Soares, A.P.Oliveira, B.Otto-Bliesner and E.Brady, 2002: Intercomparison of heat fluxes in the South Atlantic. Part 1: The Seasonal Cycle. To be published in the *Journal of Climate*.